Characterization of the surface roughness of sand particles using an advanced fractal approach

Hongwei Yang[1], Béatrice A. Baudet[1,2] and Ting Yao[1]

[1]*Department of Civil Engineering, The University of Hong Kong,*

Pokfulam Road, Hong Kong

[2]*University College London, U.K.*

Manuscript submitted to

Proceedings of the Royal Society A

[*]Corresponding author
Dr Béatrice Anne Baudet
Department of Civil, Environmental and Geomatic Engineering
University College London
Gower street
London WC1E 6BT
b.baudet@ucl.ac.uk

Abstract:

The surface roughness of soil grains affects the mechanical behaviour of soils, but the characterization of real soil grain roughness is still limited in both quantity and quality. A new method is proposed, which applies the power spectral density, typically used in tribology, to optical interferometry measurements of soil grain surfaces. The method was adapted to characterize the roughness of soil grains separately from their shape, allowing the scale of the roughness to be determined in the form of a wavevector range. The surface roughness can be characterized by a roughness value and a fractal dimension, determined based on the stochastic formation process of the surface. When combined with other parameters, the fractal dimension provides additional information about the surface structure and roughness to the value of roughness alone. Three grain sizes of a quarzitic sand were tested. The parameters determined from the power spectral density analysis were input directly into a Weierstrass-Mandelbrot function to reconstruct successfully a fractal surface.

Keywords: sand; surface roughness; fractal; power spectral density

LIST OF SYMBOLS

$A(x, y)$	auto-correlation function of surface heights
C_0	coefficient in equation (5), μm^4
C_p	coefficient to calculate G
D_{PSD}, D_{TPM}	fractal dimension determined by PSD and TPM method respectively
G	in WM function, fractal roughness, μm
$h(x, y)$	surface heights, μm
L, L_s	in WM function, largest and smallest asperity spacing or wavelength in WM, μm
M	in WM function, number of superposed ridges
n_{max}	in WM function, maximum frequency index
PSD	Power Spectral Density
q, q_1,q_0,q_c	wavevector or spatial frequency, subscripts indicate the largest, smallest and cut-off, μm^{-1}
S_a	average value of surface heights
S_q, $S_{q,roughness}$	root-mean-square value of surface heights to a mean plane for the whole measurement and for the separated roughness surface, μm
TPM	Triangular Prism Method
WM	Weierstrass-Mandelbrot

α	slope in equation (5)
γ	in WM function, density of frequencies
δ, δ_c	size of discretization in TPM method and the cut-off size, μm

INTRODUCTION

The surface of soil grains is not smooth, especially when examined at increasingly smaller scales. In the field of geotechnical engineering, surface roughness has been shown to affect the packing, shear modulus, compression and shearing behaviour of granular assemblies (Santamarina & Cascante, 1998; Yimsiri & Soga, 1999; Cavarretta *et al*., 2010; Otsubo *et al.*, 2015a; Altuhafi *et al.*, 2016), but typically these studies were made using analogue soil grains such as glass ballotini or steel balls which surface was altered by chemical or mechanical action. Characterizing the surface roughness of real soil particles, although pivotal to any quantitative analysis of its effect, remains rare (e.g. Otsubo *et al.*, 2015; Altuhafi *et al.*, 2016).

The significant role of surface roughness in the contact behaviour between objects has led to a large body of research in the fields of tribology and industrial manufacturing. In their pioneering work, Greenwood & Williamson (1966) showed that real contact surfaces with asperities have larger contact areas and smaller contact pressures than predicted by Hertz's (1881) classic solution for the elastic contact of smooth spheres. Advanced experimental imaging methods have been developed to determine accurate surface topographical information, including mechanical stylus profilometry, optical interferometry, scanning electron microscopy and atomic force microscopy. These methods are generally applied to usually flat, engineered materials

e.g. milled, sand-blasted or thin-coated. Materials investigated by interferometry tend to have good reflectivity.

In soil mechanics, there has been a growing effort to study and model the behaviour of granular geomaterials at the particle level (e.g. Cavarretta *et al.*, 2010; Senetakis *et al.*, 2013; Cundall & Strack, 1979 and subsequent DEM studies). Advances in the theory of contact mechanics of rough curved contacts, such as that proposed by Greenwood *et al.* (1984), have been used in analytical and numerical analyses of soils (Yimsiri & Soga, 2000; Scharinger *et al.*, 2008; Otsubo *et al.*, 2015a). These require a representative value of the grain surface roughness, but unlike with engineered materials, the use of some of the advanced techniques developed in other fields can be difficult to apply to soil particles, which can have a variety of shapes and roughness resulting from their mineralogy and diagenetic geological history. Depending on their mineralogy, their reflectivity can also be very low (e.g. quartzitic grains).

Sands may have diverse origins, typically clastic or bio-clastic, which has a marked effect on their nature. Some have suggested that the roughness should be a proportion of the size of the particle (e.g. Cavarretta *et al.*, 2010), which finds rationale in the effect of grain size on the processes of transportation and deposition of the soil, but the relation between the two is not obvious. Both roughness and shape are

affected by the geological origin of the grain (e.g. biogenic, erosion of igneous, metamorphic or sedimentary rock), its mineralogy and therefore hardness, but probably in slightly different ways. Particle breakage, chipping and abrasion during particle loading or transportation, perhaps related to the grain type and the transportation type (e.g. wind, water, ice) will affect the grain morphology. Particle breakage e.g. splitting may create more angular grains but depending on the mineralogy the created surfaces will be more or less smooth. For example, quartz breaks along conchoidal surfaces, while the crystalline structure of feldspar forces it to break along cleavage planes (e.g. Zhao *et al.*, 2015). On the other hand, chipping will make particles less angular. Chemical effects in the long term, which are most likely to occur after deposition, such as dissolution, either generalized or at particle contact, and modification (e.g. precipitation of iron oxide), also affect the shape and roughness in different ways. The most typically encountered materials in geotechnical engineering applications are quartz sands such as the one tested here. These have an igneous origin but which may have been through cycles and various types of weathering, erosion, transportation and deposition as a sand/sandstone so that they may have a wide range of ages.

So far characterizing soil grain surface roughness has been either by estimating the root mean square (S_q) or average (S_a) from a cut section of the grain surface (e.g. Cavarretta *et al.*, 2010; Altuhafi *et al.*, 2016), or by using two-dimensional grain

profiles obtained from scanning electron microscopy, but being able to visualize the whole grain has been at the cost of losing the resolution and significant detail of the surface roughness (e.g. Hyslip & Vallejo, 1997; Xu & Sun, 2005; Arasan *et al.*, 2011). Some studies have made successful use of advanced technology, such as optical interferometry, but the analysis of the measured data has been simplistic in comparison with the challenge of obtaining the data (e.g. Alshibli & Alsaleh, 2004; Cavarretta *et al*., 2010; Altuhafi & Coop, 2011; Senetakis *et al.*, 2013; Otsubo *et al*., 2015; Altuhafi *et al.*, 2016). The amount and quality of data on real soil particles remains small, limiting further application of the results to numerical modelling at the grain scale (e.g. in Mollon & Zhao, 2012, 2014; Hanaor *et al*., 2013, 2016; Zhou & Wang, 2015).

In order to exploit topographical measurements of soil grain surfaces better, we have adapted a method used to determine the roughness of engineered surfaces to use on particles from a natural quarzitic sand. It is found that analyzing measurement data obtained from high-resolution optical interferometry as a power spectrum can lead to a more informative yet objective quantification of roughness than currently achieved. The surface is thus described by a scale-independent parameter (the fractal dimension) in addition to the root mean square of the roughness, a suggestion that has been made for engineered surfaces (e.g. Majumdar & Tien, 1990; Zhai *et al.*, 2016a).

Several methods have been proposed in fields ranging from manufacturing to medicine to assess the fractality of surfaces. Scanning electron micrographs can be used, for example the grey scale of the images allows texture techniques to be applied, such as the "skyscraper" fractal analysis (e.g. Caldwell et al., 1990) or the "blanket" fractal analysis (e.g. Peleg et al., 1984). The projected areas of the particles, obtained from SEM or other means such as image sensor analysers, can be used with the box counting method (e.g. Buczkowski et al., 1998), or the area-perimeter method (e.g. Hyslip & Vallejo, 1997), but for soil grains high resolution images are necessary to be able to capture the surface asperities. Dividers have been used to determine the fractal dimension of surfaces, such as the triangular prism method (e.g. Clarke, 1987), variograms (e.g. Mark & Aronson, 1984), triangulation or cube-counting (e.g. Zhai *et al.*, 2016a, 2016b). Another technique is to analyse the power spectrum of the surface, for example as a Fourier power spectrum (Burrough, 1981), by power spectral density (Persson *et al.*, 2005), or as a structure function (Bushan & Majumdar, 1992). The fractality of soil grain surfaces has been suggested by researchers who have found grain contours to exhibit a self-similar or self-affine pattern down to finer scales (e.g. Orford & Whalley, 1987; Vallejo, 1995). In the following we show how natural sand grain surfaces obtained by profilometry can also be described as fractals.

TESTING APPARATUS AND TESTED SAND PARTICLES

The roughness measurements were made with a Fogale Nanotech optical microscope (model M3D 3000). FOGALE Pilot 3D software and FOGALE Viewer 3D software were used to obtain and analyse the data. The surface topography is described by an interferogram that is a function of the sample height at discrete points. The best lateral resolution that can be achieved by this interferometer is 0.184 μm (spacing of discrete points in the x and y planes perpendicular to the surface height plane $h(x, y)$), while white light profilometry ensures 3nm RMS resolution in the vertical direction. The measuring area can be up to 141.3 μm by 106.6 μm. A function available within the integrated software allows separating the shape from the roughness. The function filters separating the low frequencies associated with the shape (e.g. slope, curvatures) from the high frequencies associated with the roughness. The length of this spatial filter, also called motif size, is arbitrarily set as one quarter of the size of the field of view, and of the same unit as the image unit. The roughness is deducted by subtracting the shape from the overall surface, ensuring that the sum of the shape plus roughness is always equal to the unaltered surface (Fogale, 2009). An illustration of this decurvature process is shown in figure 1.

The tested particles are from Leighton Buzzard sand (LBS), a silica sand consisting of strong, highly spherical particles. The shape parameters were determined

by dynamic image analysis using a Qicpic image analysis sensor where soil particles are put through a vibratory feeder to disperse them before free-falling in front of pulsed light. A high speed digital camera (450 frames per second) captures images of the particles with a resolution of 1 micron for size and shape characteristics. The sphericity, calculated as the ratio of the perimeter of the grain to that of the circle of equivalent surface area, is about 0.9, and the convexity, calculated as the ratio of the surface area of the grain to the area of the convex Hull surface, is about 1.0.

There has been no systematic study of roughness of soil particles to enable determine whether their surface roughness is size dependent or not. The question of scaling i.e. whether the same value of roughness can be used throughout a range of particle sizes, for example to simulate debris flows, is however being queried by discrete element modellers. Three size groups were thus selected to try to add to the limited data available, corresponding to the sieve sizes 0.6-1.18 mm, 1.18-2mm and 2-5 mm. It was made sure by visual inspection that the particles tested were of same mineralogy (quartz). Their particle size distributions determined by dynamic image analysis are shown in figure 2. A total of 150 particles were tested, 50 for each size group. All the surface measurements were made for an area of 106.6 μm × 106.6 μm corresponding to 578 × 578 discrete points. The low reflectivity of the quartz meant that obtaining good measurements was laborious. A particular difficulty with soil

grains is that many points of the irregular surfaces cannot be measured, which are then shown on the resulting graph as fail-to-detect points or invalid pixels. The areas measured were chosen so that invalid pixels in the observed areas were less than 1%, ensuring that removal of these points by interpolation of adjacent heights data had a negligible effect. Edge effects can also be avoided in the same way. Then the surface height data for the 578 × 578 points were exported for analysis.

TEST RESULTS AND SURFACE CHARACTERIZATION

Figure 3 shows four measured surfaces for each size group. Most of the measured surfaces have a relatively spherical local shape with some small irregular dents spread on the surfaces. This is one of the main differences between natural sand surfaces and engineered surfaces where regular wavy curves often exist. By eye, there is no obvious difference between each size group apart from the surface curvature, which is more pronounced for the small grains.

It is implied from the Greenwood & Tripp (1967) solution and its variants for non-flat materials that, in order to characterize roughness, a separation procedure is needed to remove the surface curvature from the surface measurement. In optical interferometry, the motif extraction method, which was introduced by Boulanger (1992), is generally used as it is integrated in the software of the testing apparatus.

The concept of motif, introduced in metrology research in the 1970s for machinery tools manufacturing, refers to the filtering of a surface profile between regular (e.g. waviness) and irregular features associated with the roughness (Boulanger, 1992). The shape of real soil grains however does not follow a regular waviness thus measurements are very sensitive to the separation procedure (Otsubo *et al.*, 2015). For lack of better guidance the default value of the shape motif, which is available in the software and increases with the size of the measuring area, is generally chosen (Cavarretta, 2009). Another limitation of the motif extraction method applied to soils is that there is no appreciation of the scale of the asperities, and this can diminish the application of the measured roughness since the range of roughness scales is influential in the interfacial contact behavior (e.g. Goedecke *et al*., 2013; Yastrebov *et al*., 2015 for flat contacts).

For the measurements made here, the default filter length (i.e. motif size) was 26.7 mm for the measured area of 106.6 μm x 106.6 μm. This decurvature process was however only applied for comparing the values of roughness compiled with the method presented here (see figure 10 later), as the main focus of this paper is to present a new method which addresses these drawbacks and uses the whole measured dataset is unaltered (i.e. without an artificial separation of shape and roughness). Another advantage of the method, which borrows from tribology, is that instead of a

profile line we use the whole measured surface in three dimensions: x, y and h (height).

Surface morphology by Power Spectral Density (PSD)

Natural soil grains follow a stochastic forming process, which usually leads to an apparently random surface morphology. Nayak (1971) proposed to model rough surfaces as 2D, isotropic, Gaussian random processes. He represented the surface morphology by using a spectrum, which can reveal periodic surface features that might otherwise appear random. The power spectral density is calculated by:

$$\mathrm{PSD}(q_x, q_y) = \frac{1}{(2\pi)^2} \iint_{-\infty}^{\infty} A(x,y) e^{-i(xq_x + yq_y)} \mathrm{d}x\mathrm{d}y \quad (1)$$

where $A(x, y)$ is the auto-correlation function of surface heights $h(x, y)$ and q is the wavevector or spatial frequency (in μm^{-1}). By using the PSD, the spatial surface heights data are transferred into the spatial frequency or wavevector domain through a discrete Fourier transform. In order to facilitate the interpretation of the surfaces, a routine angular averaging is performed where the surface is assumed to be isotropic so that the PSD(q_x, q_y) reduces to PSD(q) and is independent of x or y direction (Nayak, 1971). This assumes that the PSD is the same along the x and y direction. Figure 4(a) shows the PSDs in each in-plane direction, averaged over 289 x-profiles and 289 y-profiles, together with the angular averaged PSD. The average PSDs in both

in-plane directions are almost coincident, indicating no major anisotropy as can be found in some manufactured surfaces (e.g. Majumdar & Tien, 1990). The angular averaged PSD is taking into account all the measurements and therefore not necessarily equal to the average of the two PSDs in x- and y-directions.

Figure 4(b) shows the PSDs for all the 2-5 mm particles, using the angular average PSD (referred to thereafter simply as PSD). No spike or jump is observed, indicating that there is no predominant wavevector in those surfaces. Each PSD curve contains information both about the local shape, at small wavevectors, and the roughness, at large wavevectors, thus potentially enabling the characterization of roughness and shape separately but more objectively than the routine motif method. The variation in PSD within the same size group indicates different roughnesses for different grains, and the average PSD is also shown. The zeroth, second and fourth moments of the PSD relate to physical statistical parameters of the surface (Nayak, 1971). For example, the zeroth moment of the PSD relates to S_q and can be expressed as (Nayak, 1971; Persson *et al.*, 2005):

$$S_q = \left(2\pi \int_{q_0}^{q_1} \mathrm{PSD}(q) q \, \mathrm{d}q\right)^{0.5} \quad (2)$$

where q_0 and q_1 denote the smallest and largest wavevectors of the measured surface respectively. Here we take the values suggested by Persson *et al.* (2005): $q_0 = \frac{2\pi}{L}$, with L = 106.6 μm (size of the measured area) and $q_1 = \frac{N}{2}\frac{2\pi}{L}$, with L/N = 0.184 μm

(resolution). Figure 5(a) shows the comparison between the values of S_q obtained from the PSD after angular averaging and from statistics using:

$$S_{\mathrm{q}} = \left(\frac{1}{XY}\sum_{i=1}^{X}\sum_{j=1}^{Y} h(i,j)\right)^{0.5} \quad (3)$$

The values are in very good agreement, with an error less than 0.1% (0.001μm). This validates the calculation of the PSD and shows that the angular averaging which assumes the surface to be isotropic has a negligible effect on the parameters. A similar graph obtained for different sizes of field of view taken on a grain of size 0.6-1.18 mm, shown in figure 5(b), indicates that the size of the field of view (i.e. the value of L) does not affect the good comparison between the values of S_q derived from PSD and from the motif method.

The value of S_q derived with the PSD takes account of the whole measured surface, unaltered, as it takes all wavevectors into account, and therefore encompasses both shape and roughness. The high values of S_q, between 2 and 20 μm, capture mainly the shape of the grains, even more so in the smaller particles, resulting in larger roughness values for those.

In order to determine the value of the roughness alone, which we call $S_{q,roughness}$, the scales at which the roughness acts and at which the shape acts should be determined. We describe below how we simply use a cut-off wavevector, q_c, that relates to the largest wavelength that contributes to the surface roughness, to separate

roughness and shape in the PSD. The value of q_c depends on the particular surface measured and therefore should vary from particle to particle.

SEPARATION BETWEEN SHAPE AND ROUGHNESS SURFACES

Determination of the cut-off vector q_c

As a first step the sensitivity of the value of the surface roughness $S_{\text{q,roughness}}$ to the cut-off wavevector q_c is investigated. Figure 6 shows the three average PSD curves for the three size grain groups, with four different values of q_c for wavelengths between 1.3 and 5.3 microns. According to equation (1), by replacing q_0 with q_c, i.e. only considering the data between q_c and q_1, we should obtain the value $S_{q,roughness}$. Increasing q_c four times has the effect to reduce the value of $S_{\text{q,roughness}}$ by up to 48% (table 1), thus, although more suited to soil grains than the motif extraction, caution should be taken when determining q_c to obtain a reliable value of roughness.

We use the idea that the surface area calculated by discretizing into a grid, which will increase as the grid mesh size decreases, should show a marked increase when features associated with the roughness of the surface are captured by the grid. The surface area is estimated geometrically using the Triangular Prism method (TPM) (Clarke, 1986). The TPM being more suitable for self-similar surfaces (De Santis et al.,

1997), which occur rarely in nature (e.g. Shelberg et al., 1983), here we use it primarily as a means to separate shape and roughness. Figure **7** shows a visual illustration of a typical surface that is discretized with mesh sizes δ proportional to the resolution: [64, 48, 16, 10, 4, 1] × 0.184 μm. The smaller the δ, the more the discretized surface will match the measured surface. Figure 8(a) shows the estimated surface area changes with grid sizes of [64, 48, 24, 16, 10, 8, 6, 5, 4, 3, 2, 1] × 0.184 μm, for grains 2-5 mm, using a finer grid around 2 μm in order to determine the cut-off size delimiting shape from roughness and to provide more information in the small δ region. Using finer grids, for example the finest [64: -1:1] (i.e. [64, 63, 62, …, 3, 2, 1] x 0.184 μm), would lead to highly fluctuating values of surface area, as shown in figure 8(b). The estimated surface area decreases slowly down to about δ = 1.84 μm, accelerating as grid sizes decrease from 1.84 μm to 0.184 μm. This may indicate that asperities of surface roughness enter the surface area estimation for those small grid sizes. This is consistent with the suggestion that the morphology of irregular particles might be best described over two fractal subsets characterizing the texture (≈ roughness) and structure (≈ shape) (e.g. Orford & Whalley, 1987; Bhushan & Majumdar, 1992; Hyslip & Vallejo, 1997). The grid size $\delta_c \approx 1.84$ μm, regarded as the maximum size of asperity or the minimum wavelength, is taken to be the cut-off grid size between shape and roughness, the smaller grid sizes defining the roughness. The parameter δ_c,

does not change with particle size for the sand and size range investigated and represents between 0.06% and 0.3% of the dimension of the soil grains.

The values of $S_{q,roughness}$ are calculated using the PSD (equation (2)), with a lower cut-off value of $q_c \approx 2\pi/\delta_c = 3.42\ \mu m^{-1}$ determined from the estimated surface area above. They are plotted in Figure 9. For the two larger sized grains, the majority of the roughness values is between 0.35 and 0.45 microns, while the smaller grains have values of roughness varying over a larger range. The distributions are not normal and they are more peaked for the larger particles. The average value is 0.66 (±0.29) μm, 0.46 (±0.14) μm and 0.36 (± 0.08) μm for particles of sizes from 0.6-1.18 mm, 1.18-2 mm and 2-5 mm respectively i.e. while δ_c does not change with particle size, S_q does. Cavarretta *et al*. (2010) reported values of $S_{q,roughness}$ for LBS sand grains of 0.7–2.2 mm diameter of 0.3 μm and Senetakis *et al*. (2013) reported 0.38 (±0.124) μm for grains of 1.18-5 mm. In both cases the measured areas were smaller, which might affect their results (Cavarretta, 2009; Otsubo *et al.*, 2015), and the motif extraction method was used. Otsubo *et al.* (2015) showed that the standard deviation increases with reducing size of the measuring area. The values obtained from the PSD method and the motif extraction method using the default input value in the software (shape motif of 26.7 microns) are compared in figure 10: for the small particle sizes (0.6-2 mm) the motif extraction method underestimates $S_{q,roughness}$, which indicates that a

smaller value of δ_c than 1.84 μm, i.e. a smaller roughness scale, was used in the motif method, while for the larger particle sizes the motif extraction method gives a higher value of $S_{q,roughness}$, indicating that a larger roughness scale was used. The value of the motif depends on the size of the measured area, independently of the material tested, while the cut-off wavelength has a physical relation to the surface of the grains tested. In that sense, even if sometimes the values from the two methods are comparable, the method presented here gives more control and physical meaning over the value of $S_{q,roughness}$.

FRACTAL APPROACH TO CHARACTERIZE SURFACE ROUGHNESS

The morphology of soil grains can be characterized successfully by fractal dimensions (e.g. Orford & Whalley, 1987; Vallejo, 1995), which can be used to recreate realistic numerical models of surfaces (e.g. Hanaor *et al.*, 2013). Several researchers have proposed and compared different methods for the fractal analysis of surfaces e.g. Sun *et al*. (2006) and Lopes & Betrouni (2009). Here we use and compare two methods: the PSD method, based on the stochastic formation process, and the TPM, based on the geometry of the surface. The PSD method is suited to natural surfaces, which typically exhibit different scales in the vertical and in-plane directions (e.g. Xu et al., 1997) while the TPM should be most suited to self-similar surfaces (e.g. De Santis et

al., 1997). It is therefore expected that the TPM may not be as conclusive as the PSD method to characterise the surface of natural soil grains. Unlike in previous studies of soil grains, which were carried out on the profile of the particles, here the analysis was performed on 3D surfaces.

The surface area calculated by the TPM method, if fractal, is related to the grid size by (Clarke, 1986):

$$S \ \ (\delta_c > \delta) \sim \delta^{2-D_{\mathrm{TPM}}} \tag{4}$$

where D_{TPM} is the fractal dimension determined by TPM. Figure 11(a) shows the averaged surface area against grid size for each size group. The slopes of the lines, equal to 2 - D_{TPM}, decrease with increasing grain size, indicating an increase in D_{TPM} with particle size and therefore an increase in the estimated real surface area for higher fractal dimensions. Average curves are shown to highlight the trends. The distribution of D_{TPM} values obtained from all the measurements is reported in figure 11(b). The values of D_{TPM} for sizes 0.6-1.18 mm are slightly higher than those for 1.18-2 mm while the values for sizes 2-5 mm are much smaller than the other two size groups. The distributions of D_{TPM} have the same trend as the distribution of $S_{\mathrm{q,roughness}}$, which might be expected as the method is based on the graphical representation of the surface and a rougher surface is usually accompanied with a higher surface area, but here the distribution for the smaller particles is narrower. Zhai *et al.* (2016a) also

found on aluminium disks treated by mechanical attrition that the fractal dimension compiled by triangulation or cube-counting and the RMS roughness have similar trends, although in their case the roughness was higher for the larger particles.

Similarly, a fractal surface would imply that the PSD follows a power law when $q > q_c \approx 3.42\ \mu m^{-1}$, with the slope of the spectrum related to the fractal dimension. This is expressed as:

$$\mathrm{PSD}(q \geq q_c) = C_0\left({}^{q}/_{q_c}\right)^{\alpha} \quad (5)$$

where α (<0) is the slope of the straight fitting line in the double logarithmic plane of PSD versus q, and C_0 is related to the intercept. The fractal dimension, D_{PSD}, can be expressed in terms of α, and several relationships have been proposed: Voss (1988) and Turcotte (1997) adopted the relationship $D_{\mathrm{PSD}} = 4 + \alpha/2$ for a 3D surface, with D_{PSD} the fractal dimension determined by PSD. For fractal surfaces generated using Weierstrass-Mandelbrot functions, the relationship $D_{\mathrm{PSD}} = 2.5 + \alpha/2$ was adopted by Majumdar & Bhushan (1990) for 2D surfaces and $D_{\mathrm{PSD}} = 3.5 + \alpha/2$ was adopted e.g. by Liou & Lin (2006) for 3D surfaces.

Figure 12(a) shows the fractal parameters D_{PSD} calculated with $D_{\mathrm{PSD}} = 3.5 + \alpha/2$ from the averaged PSDs for each size group; the distributions of D_{PSD} for all particles are shown in figure 12(b). The values of D_{TPM} and D_{PSD} for a given particle size are distributed differently**.** It is found that D_{PSD} increases with increasing particle

size, which shows an opposite trend to D_{TPM} and $S_{q,roughness}$. The closer fit to a linear equation for the PSD data (figure 12(a)) compared to the surface area data (figure 11(a)) seems to indicate that the surfaces satisfy self-affinity rather than self-similarity implied by the TPM.

If the fractal rule applies, combining equations (2) and (5) leads to:

$$S_{\mathrm{q,roughness}} = \left(2\pi \frac{{q_c}^2 C_0}{\alpha+2}\left(\left({q_1}/{q_c}\right)^{\alpha+2} - 1\right)\right)^{0.5} \quad (6)$$

which depends on the values of the coefficient C_0, the fractal dimension D_{PSD} as well as q_c/q_1 and q_c. If we plot the values of $S_{q,roughness}$ determined from the PSD (equation (2)) against those of C_0 (figure 13), we can define a unique relationship between the two parameters which can be described as:

$$S_{q,roughness} = a C_0^b \quad (7)$$

with a = 5.95 and b = 0.41 the best-fitting values. There is a slight deviation from equation (6), for which the exponent of C_0 is equal to 0.5. Deriving $S_{q,roughness}$ from equation (6) with the average values of D_{PSD} and C_0 in figure 13 gives consistently lower values than when using equation (2) (table 1). The values of C_0 associated with the average values of D_{PSD}, also in table 2, reflect the change in roughness as well. The fractal dimensions may depend on the resolution since the measured surface heights are sampled at discrete lengths, but the hierarchical structure of the surface evidenced by the straight lines in the roughness range may be independent of the instrument

resolution. Persson (2014) showed that the slope of the linear part of the PSD obtained from several testing methods with resolution ranging in magnitude from around 100 to 0.01 μm is rather consistent.

An example of reconstructed surfaces using the obtained parameters

Numerous studies have shown the strong dependence of interfacial mechanical properties on the PSD, the value of D_{PSD}, or the range of roughnesses for flat surfaces (e.g. Akarapu *et al*., 2010; Hanaor *et al.*, 2013). The Weierstrass-Mandelbrot (WM) function and its variants can be used to reconstruct and analyze self-affine surfaces (e.g. Hanaor *et al.*, 2013), but the identification of the input parameters can be a difficult task. A realistic reproduction of the surface relies on realistic input parameters. Following Majumdar & Bhushan (1990) and Yan & Komvopoulos (1998), we use the parameters determined from the PSD of the soil surface to reconstruct the surfaces using a variant of the Weierstrass-Mandelbrot function proposed by Yan & Komvopoulos (1998). The parameters determined experimentally above are input directly where possible. The WM function is expressed as:

$$h(x,y) = L\left(\frac{G}{L}\right)^{D_{PSD}-2}\left(\frac{\ln\gamma}{M}\right)^{0.5}\sum_{m=1}^{M}\sum_{0}^{n_{\max}}\gamma^{n(D-3)}\left\{\cos\psi_{m,n} - \cos\left[\frac{2\pi\gamma^{n}\left(x^2+y^2\right)^2}{L}\cos\left(\tan^{-1}\frac{y}{x}-\frac{2\pi m}{M}\right) + \cos\psi_{m,n}\right]\right\} \quad (8)$$

where the length factor of the highest asperity spacing, or sample wavelength, L, is

taken as δ_c = 1.84 μm, the smallest length is L_s=0.184 μm and a parameter related to the density of frequencies, γ, is set to a commonly adopted value of 1.5, which leads to the maximum frequency index n_{max} = 6. The number of superposed ridges used to construct the surface, M, is not a first-order parameter (Yan & Komvopoulos, 1998) and is set to be 20 to make the surface structure sufficiently random. The influential parameters are D_{PSD}, taken as the average values of 2.22, 2.37, 2.41 for the three grain sizes (figure 11a), and the associated coefficient C_0 =6.3x10^{-3} μm^4, 2.4 x10^{-3} μm^4 and 1.3x10^{-3} μm^4. The fractal roughness, G, can be calculated from Liou & Lin (2006):

$$G = \left(\frac{C_p \cdot \sin\left(\frac{\pi(2D-5)}{2}\right)\Gamma(2D-5)}{(3-D)2^{2(4-D)}\ln\gamma} \right)^{1/(2D-4)} \quad (9)$$

with C_p= C_0 $q_c^{-\alpha}$. Values of G equal to 6.0 x10^{-3} μm, 8.3 x10^{-3} μm and 6.3 x10^{-3} μm are found for the three grain sizes respectively in increasing size order. $\varphi_{m,n}$ is the random phase angle and is chosen so that the equivalent fractal surfaces have roughness values $S_{q,roughness}$ equal to 0.70 μm, 0.48 μm and 0.37 μm, in order of increasing grain size. The reconstructed surfaces are of area 9.2 μm× 9.2 μm, so they fit within the bounds of the cut-off grid size and should be dominated by roughness (figure 14(a)). They represent a portion of the measured area, and although flat it would be possible to wrap it on a shape as shown by e.g. Liou *et al.* (2010) or Hanaor *et al.* (2016) who modified the WM to overlay a planar rough surface onto a sphere.

The WM surfaces were reconstructed while controlling their roughness to be the same $S_{q,roughness}$ as the real sand particles tested. Their small area ensured that the shape was not affecting the comparison between the measured and reconstructed roughness surfaces (figure 14(b)). Some differences are observed in the location and heights of the asperities, but although reconstructing the complex surface of a soil grain exactly as it is may not be possible, there is a statistical resemblance. This highlights one of the problems with determining the surface roughness of sand grains, which is that no two grain surfaces are the same. The limited size of the measuring areas, which despite being the largest possible in this paper is still much smaller than the whole grain surface, is also a drawback. It seems likely that the variation in surface roughness on a given grain may be less than the variation in shape, but one should be aware of these limitations when using the measured data.

CONCLUSIONS

A method to characterize the surface roughness of soil grains is proposed. The power spectral density, a powerful tool to reveal the periodic feature of a random surface which is typically used in tribology, was adapted to characterize the surface roughness of soil grains separately from their shape, a procedure less straightforward than for engineered surfaces. The scale of the roughness, information usually missing in other

methods of determining soil grain roughness, was quantified in the form of a wavevector range determined from the estimation of the surface area by triangular-prism method. The surface roughness was then characterized over that range using the power spectral density.

For three sizes of quarzitic sand particles considered here, the surface roughness has been characterized by a roughness value, $S_{q,roughness}$, and a fractal dimension, determined from the power spectral density (D_{PSD}), which is more suitable for natural surfaces where different scales exist in the vertical and in-plane directions. The D_{PSD}, when combined with other parameters, such as the coefficient C_0 from the PSD, carries more information about the surface structure and roughness than the value of roughness alone.

The obtained data contribute to the current very limited database on real soil particles, with potential use in numerical modelling for creating numerical particles and simulating interfacial grain contacts. A variant of Weierstrass-Mandelbrot function was used successfully to reconstruct a fractal surface with the parameters identified experimentally as direct input.

DATA ACCESSIBILITY

Surface data measured by interferometry on fifteen particles (five for each size) and

which support this article can be accessed at http://discovery.ucl.ac.uk/1508516/.

AUTHORS' CONTRIBUTIONS

The first author collected some surface data, performed the analyses and drafted the manuscript. The third author collected a large amount of surface data and has contributed to some figures. Both were working under the second author's supervision. All authors have read and approved the final version of the paper.

COMPETING INTERESTS

There are no competing interests in this research.

FUNDING

The authors acknowledge the financial support provided by the Research Grants Council (RGC) of HKSAR (grants GRF 17200114 and TR22-603-15N).

ACKNOWLEDGEMENTS

Professor BNJ Persson is gratefully acknowledged for helping with early calculations of the PSD and for his advice. We also would like to thank Professor Matthew Coop and Professor Jidong Zhao for fruitful discussions.

REFERENCES

Akarapu, S., Sharp, T. & Robbins, M.O. 2011 Stiffness of contacts between rough surfaces. *Physical Review Letter* **106**, 204301.

Alshibli, K.A. & Alsaleh, M.I. 2004 Characterizing surface roughness and shape of sands using digital microscopy. *Journal of Computing in Civil Engineering* **18**, 36-45.

Altuhafi, F.N. & Coop, M.R. 2011 Changes to particle characteristics associated with the compression of sands. *Géotechnique* **61**(6), 459-471.

Altuhafi, F., Coop, M.R. & Georgiannou, V.N. 2016 Effect of particle shape on the mechanical behaviour of natural sands. *International Journal of Geotechnical and Geoenvironmental Engineering.*

Arasan, S., Akbulut, S. & Hasiloglu, A.S. 2011 The Relationship between the Fractal Dimension and Shape Properties of Particles. *KSCE Journal of Civil Engineering* **15**(7),1219-1225

Boulanger, J. 1992 An interesting complement to ISO parameters for some functional problems. International Journal of Machine Tools and Manufacture 32(1/2), 203-209.

Buczkowski. S., Hildgen, P. & Cartilier, L. 1998 Measurements of fractal dimension by box-counting: a critical analysis of data scatter. Physica A 252(1-2), 23-34.

Burrough, P.A. 1981 Fractal dimensions of landscapes and other environmental data. Nature 295, 240-242.

Bushan, B. & Majumdar, A. 1992 Elastic-plastic contact model for bifractal surfaces. Wear 153, 53-64.

Caldwell, C.B., Stapleton, S.J., Holdsworth, D.W., Jong, R.A., Weiser, W.J., Cooke, G. *et al.* 1990 Characterization of mammographic parenchymal pattern by fractal dimension. Phys Med Biol. 35, 235-247.

Cavarretta, I. 2009 *The influence of particle characteristics on the engineering behaviour of granular materials*, PhD thesis, Department of Civil and Environmental Engineering, Imperial College London.

Cavarretta, I., Coop, M. & O'Sullivan, C. 2010 The influence of particle characteristics on the behaviour of coarse grained soils. *Géotechnique* **60**(6), 413-423.

Clarke, K.C. 1986 Computation of the fractal dimension of topographic surfaces using the triangular prism surface area method. *Computers and Geosciences* **12**(5), 713–722.

Cundall, P.A. & Strack, O.D.L. 1979 A discrete numerical model for granular assemblies. *Géotechnique* **29**(1), 47-65.

De Santis, A., Fedi, M. & Quarta, T. 1997 A revisitation of the triangular prism surface method for estimating the fractal dimension of fractal surfaces. Annali di Geofisica XL(4), 811-821.

Fogale (2009). Fogale nanotech user manual version 2.2.1. Nimes, France: Fogale.

Goedecke, A., Jackson, R.L. & Mock, R. 2013 A fractal expansion of a three dimensional elastic–plastic multi-scale rough surface contact model. Tribology International 59,230-239.

Greenwood, J.A. & Williamson, J.B.P. 1966 Contact of Nominally Flat Surfaces. Proceedings of the Royal Society of London. Series A: Mathematical and Physical Sciences 295(1442): 300-319.

Greenwood, J.A. & Tripp, J.H. 1967 Elastic Contact of Rough Spheres. ASME Journal of Applied Mechanics 34(1), 153-159.

Greenwood, J.A., Johnson, K. & Matsubara, E. 1984 A surface roughness parameter in Hertz contact. Wear 100(1–3), 47-57.

Hanaor, A.H., Gan, Y. & Einav, I. 2013 Effects of surface structure deformation on static friction at fractal interfaces. Géotechnique Letters 3(2), 52-58.

Hanaor, A.H., Gan, Y., Revay, M., Airey, D.W. & Einav, I. 2016 3D printable geomaterials. Géotechnique 66(4), 323-332.

Hertz, H. 1881 On the contact of elastic bodies. Journal für die reine und angewandte Mathematic 92, 156-171. (in German)

Hyslip, J.P. & Vallejo, L.E. 1997 Fractal analysis of the roughness and size distribution of granular materials. Engineering Geology 48, 231-244.

Liou, J.L. & Lin, J.F. 2006 A New Method Developed for Fractal Dimension and Topothesy Varying With the Mean Separation of Two Contact Surfaces. Journal of Tribology 128, 515-524.

Liou, J.L., Tsai, C.M. & Lin, J.F. 2010 A microcontact model developed for sphere- and cylinder-based fractal bodies in contact with a rigid flat surface. Wear 268, 431-442.

Lopes, R. & Betrouni, N. 2009 Fractal and multifractal analysis: A review. Medical Image Analysis 13, 634–649.

Majumdar, A. & Bhushan, B. 1990 Role of Fractal Geometry in Roughness Characterization and Contact Mechanics of Surfaces. ASME Journal of Tribology 112(2), 205-216.

Majumdar, A. & Tien, C. 1990 Fractal characterization and simulation of rough surfaces. Wear 136, 313-327.

Mark, D.M. & Aronson, P.B. 1984 Scale-dependent fractal dimensions of topographic surfaces: an empirical investigation, with applications in geomorphology and computer mapping. Mathematical Geology 16(7), 671-683.

Mollon, G. & Zhao, J. 2012 Fourier–Voronoi-based generation of realistic samples for discrete modelling of granular materials. Granular Matter 14, 621-638.

Mollon, G. & Zhao, J. 2014 3D generation of realistic granular samples based on random fields theory and Fourier shape descriptors. Computer Methods in Applied Mechanics and Engineering 279, 46-65.

Nayak, P.R. 1971 Random Process model of rough surfaces. Journal of Lubrication Technology 93(3), 398-407.

Orford, J.D. & Whalley, W.B. 1987 The quantitative description of highly irregular sedimentary particles: the use of the fractal dimension. In: Clastic particles. Scanning electron microscopy and shape analysis of sedimentary and volcanic clasts (J.R. Marshall ed.), pp. 267-280. New York: Van Nostrand Reinhold Co.

Otsubo, M, O'Sullivan, C. & Sim, W.W. 2015 A methodology for accurate roughness measurements of soils using optical interferometry. In: Geomechanics from micro to macro, Proceedings IS-Cambridge 2014 (K. Soga, K. Kumar, G. Biscontin and M. Kuo eds.), pp. 1117-1122. London, UK: CRC Press.

Otsubo, M, O'Sullivan, C., Sim, W. W. & Ibraim, E. 2015a Quantitative assessment of

the influence of surface roughness on soil stiffness. Géotechnique 65(8), 694-700.

Peleg, S., Naor, J., Hartley, R. & Avnir, D. 1984 Multiple resolution texture analysis and classification. IEEE Trans. Pattern Anal. Mach. Intell. 6, 518-523.

Persson, B.J.N., Albohr, O., Tartaglino, U., Volokitin, A.I. & Tosatti, E. 2005 On the nature of surface roughness with application to contact mechanics, sealing, rubber friction and adhesion. J. Phys.: Condens. Matter 17, R1-R62. doi:10.1088/0953-8984/17/1/R01.

Persson, B.N.J. 2014 On the Fractal Dimension of Rough Surfaces. Tribology Letter 54, 99-106.

Santamarina, C. & Cascante, G. 1998 Effect of surface roughness on wave propagation parameters. Géotechnique 48(1), 129-136.

Scharinger, F., Schweiger, H.F. & Pande, G.N. 2008 On a multilaminate model for soil incorporating small strain stiffness. International Journal for Numerical and Analytical Methods in Geomechanics 33(2), 215–243.

Senetakis, K., Coop, M.R. & Todisco, C.M. 2013 The inter-particle coefficient of friction at the contacts of Leighton Buzzard sand quartz minerals. Soils and Foundations 53(5), 746-755.

Shelberg, M.C., Lam, N. & Moellering, H. 1983 Measuring the fractal dimensions of

surfaces. Proc. Automated Cartography 6, 319-328.

Sun, W., Xu, G., Gong, P. & Liang, S. 2006 Fractal analysis of remotely sensed images: A review of methods and applications. International Journal of Remote Sensing 27(22), 4963–4990.

Turcotte, D.L. 1997 Fractals and chaos in Geology and Geophysics. Cambridge University Press.

Voss, R.F. 1988 In: Fractals in nature: From characterization to simulation (H.O. Peitgen HO and D. Saupe eds), pp. 21-70. New York: Springer-Verlag.

Vallejo, L.E. 1995 Fractal analysis of granular material. Géotechnique 45(1), 159-163.

Xu, T., Moore, I.D. & Gallant, J.C. 1993 Fractals, fractal dimensions and landscapes – a review. Geomorphology 8, 245-262.

Xu, Y.F. & Sun, D.A. 2005 Correlation of surface fractal dimension with frictional angle at critical state of sands. Géotechnique 55(9), 691–695.

Yan, W. & Komvopoulos, K. 1998 Contact analysis of elastic-plastic fractal surfaces. Journal of Applied Physics 84(7), 3617-3624.

Yastrebov, V.A., Anciaux, G. & Molinari, J.F. 2015 From infinitesimal to full contact between rough surfaces: Evolution of the contact area. International Journal of Solids and Structures 52, 83-102.

Yimsiri, S. & Soga, K. 2000 Micromechanics-based stress±strain behaviour of soils at small strains. Géotechnique 50(5), 559-571.

Zhai, C., Gan, Y., Hanaor, D., Proust, G. & Retraint, D. 2016a The Role of Surface Structure in Normal Contact Stiffness. Experimental Mechanics 56, 359-368.

Zhai, C., Hanaor, D., Proust, G., Brassart, L. & Gan, Y. 2016b Interfacial electro-mechanical behaviour at rough surfaces. Extreme Mechanics Letters.

Zhao, B., Wang, J., Coop, M.R., Viggiani, G. & Jiang, M. 2015 An investigation of single sand particle fracture using x-ray mico-tomography. Géotechnique 65(8), 625-641.

Zhou, B. & Wang, J. 2015 Random generation of natural sand assembly using micro x-ray tomography and spherical harmonics. Géotechnique letters 5(1), 6-11.

Table 1 Variation of $S_{q,roughness}$ with different cut-off wavevectors q_c

Particle size, mm	q_c, μm^{-1}			
	1.18	2.36	3.42	4.72
0.6-1.18	1.19	0.86	0.72	0.62
1.18-2.36	0.75	0.56	0.49	0.43
2.36-5	0.56	0.43	0.37	0.33

Table 2 Comparison of values of $S_{q,roughness}$ computed using equation 6 and equation 2. The values of D_{PSD} and C_0 are also shown in the table.

Particle size range, mm	Averaged $S_{q,roughness}$, μm		D_{PSD}	C_0, μm^4			
	From Eq. 6	From Eq. 2	Mean	Mean	Min.	Max.	Std.
0.6-1.18	0.70	0.72	2.21	6.3E-03	6.7E-04	4.8E-02	8.0E-03
1.18-2	0.48	0.49	2.37	2.4E-03	5.1E-04	9.3E-03	2.0E-03
2-5	0.37	0.37	2.41	1.3E-03	3.9E-04	4.0E-03	8.4E-04

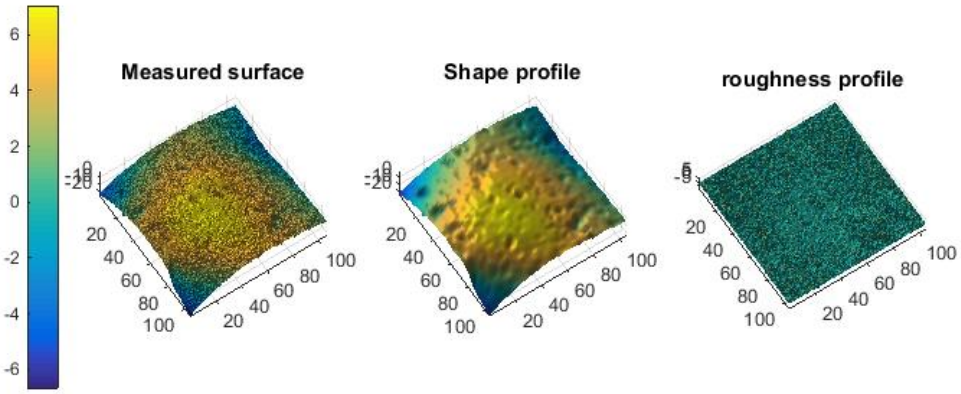

Figure 1 Illustration of separation of shape and roughness by the software integrated in the interferometer

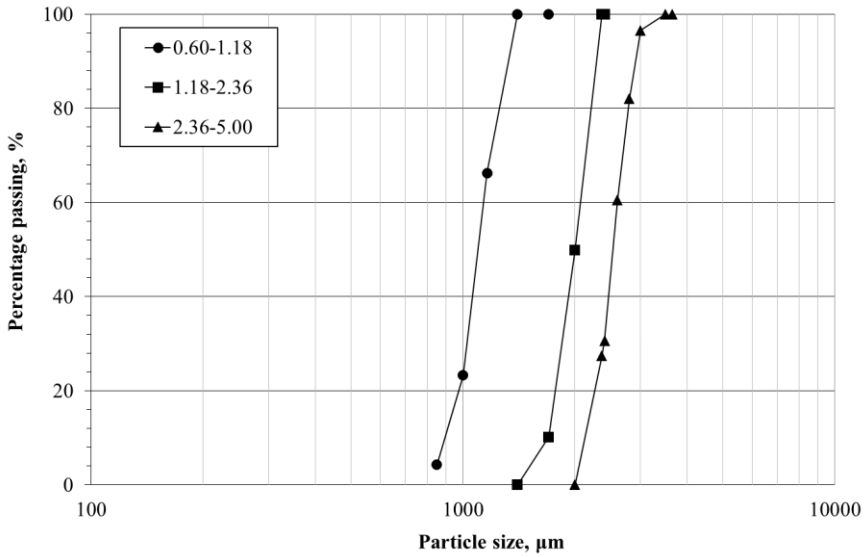

Figure 2 Particle size distributions for the three size groups

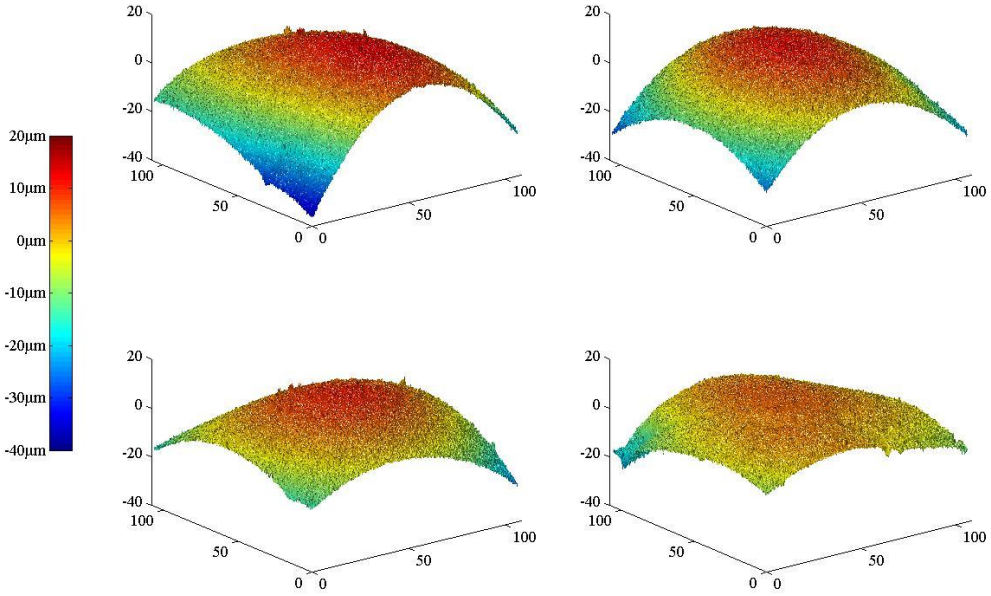
20μm
10μm
0μm
-10μm
-20μm
-30μm
-40μm
20
0
-20
-40
100
50
0
0
50
100

(a)

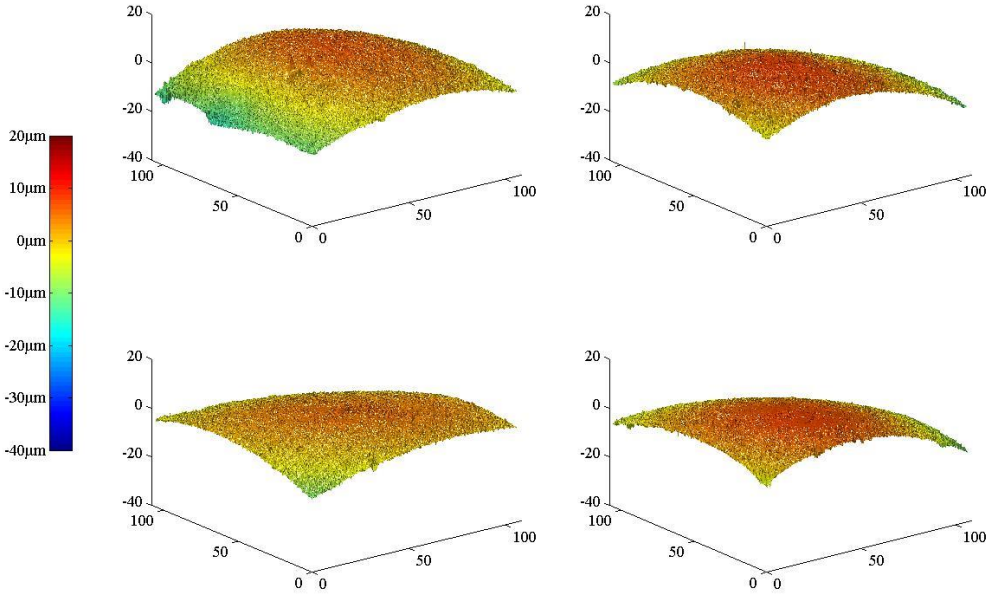
20μm
10μm
0μm
-10μm
-20μm
-30μm
-40μm
20
0
-20
-40
100
50
0
0
50
100

(b)

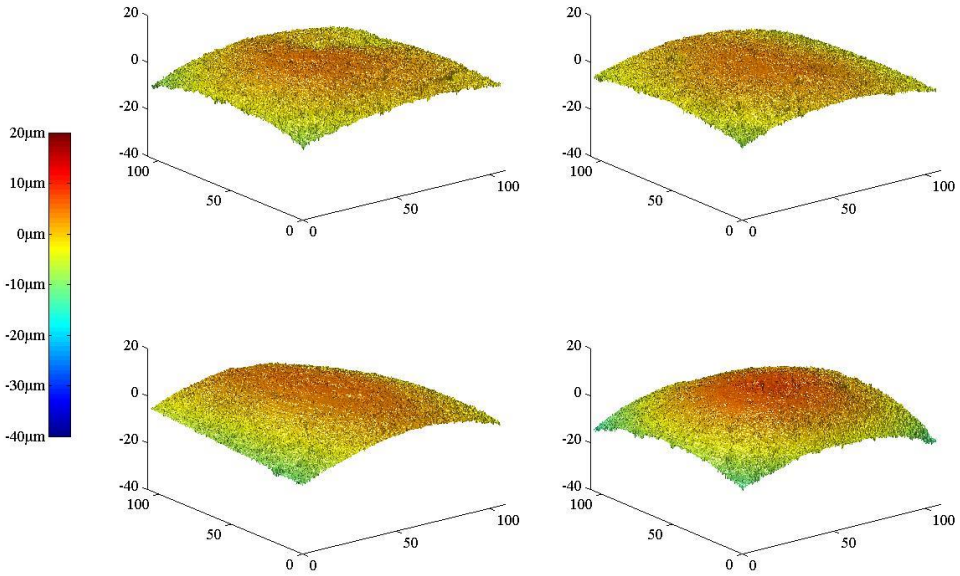

(c)

Figure 3 Images of the measured surface for particles of size (a) 0.6-1.18 mm, (b) 1.18-2 mm, (c) 2-5 mm

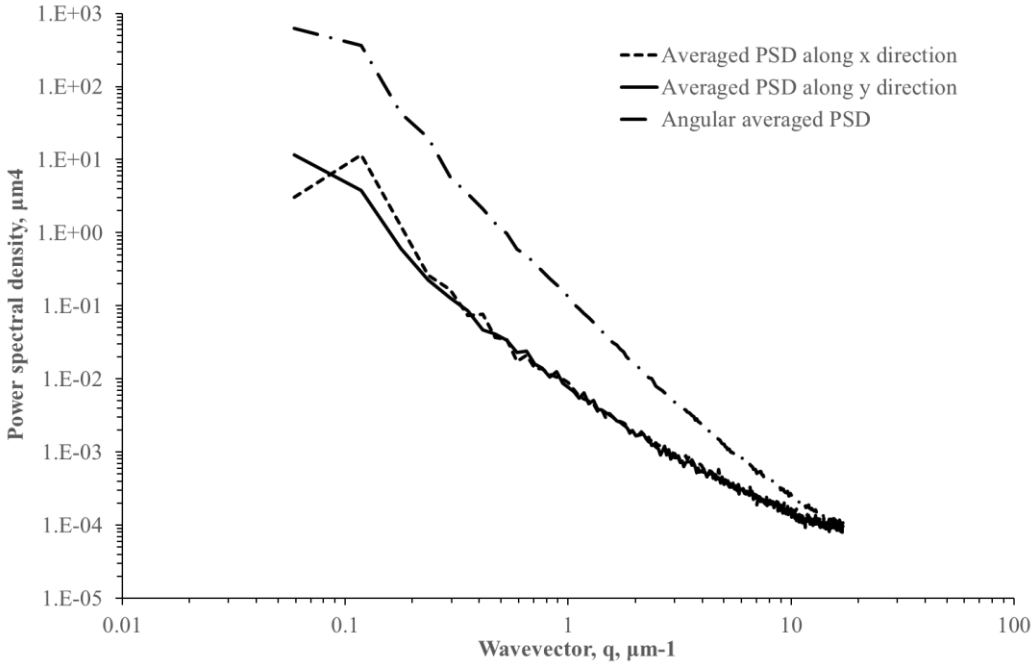

(a)

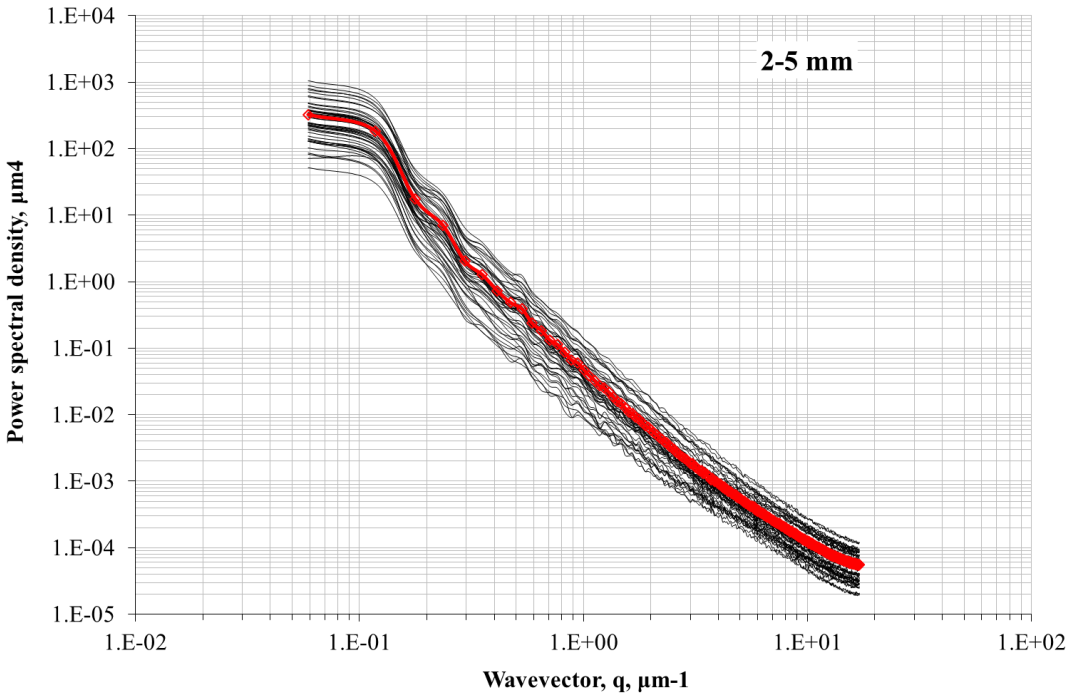

(b)

Figure 4 Power Spectrum Density **(a) comparison of PSD in x- and y-directions**; (b) angular averaged PSD for particles of size 2-5 mm. The average PSD group is indicated by the bold red line.

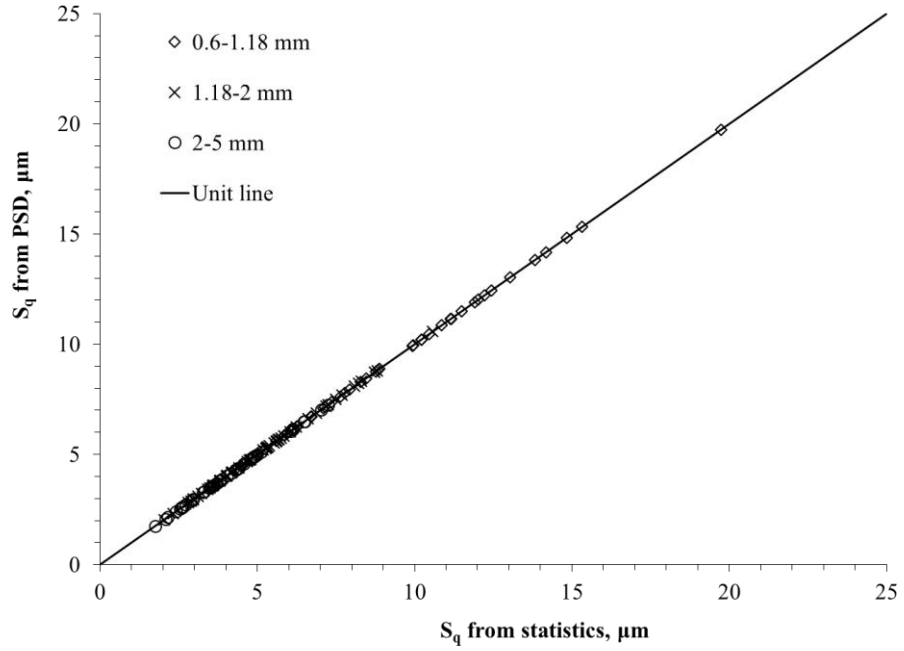

(a)

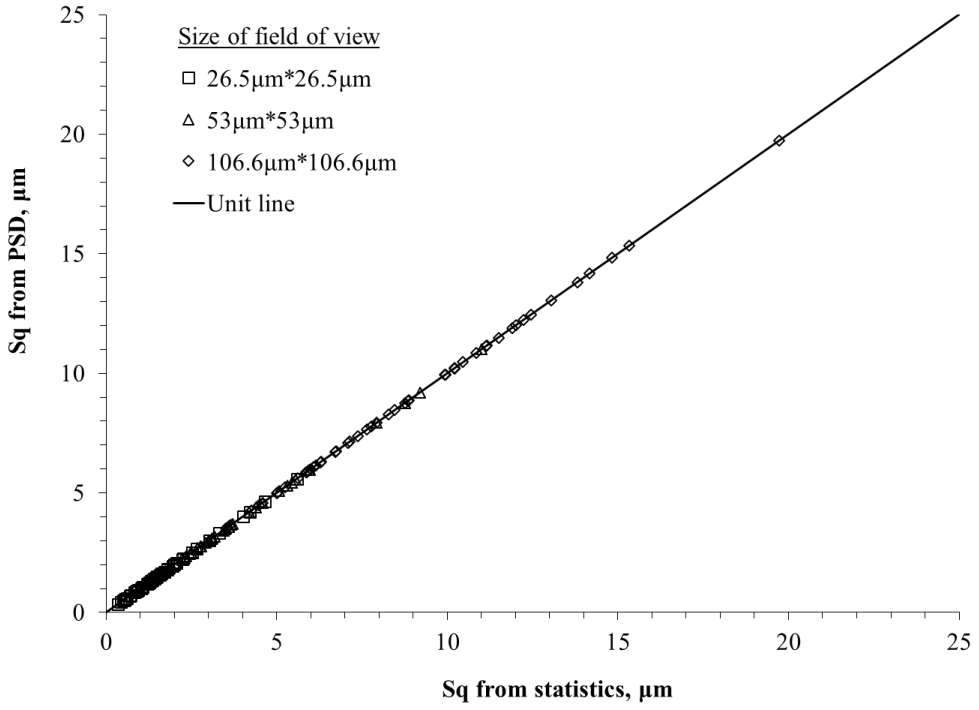

(b)

Figure 5 Comparison of roughness values S_q for whole surface measurements obtained from PSD (equation 2) and statistics (equation 3) (a) for different particle sizes, **(b) for different sizes of field of view (grain size 0.6-1.18 mm)**

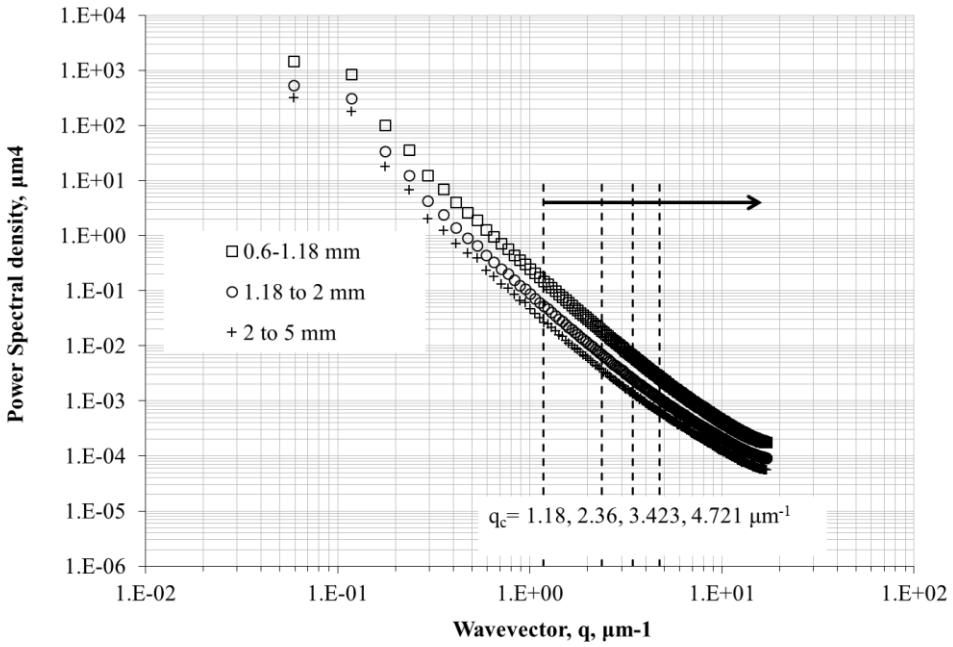

Figure 6 Illustration of changing cut-off wavelength on the PSD for the three particle sizes

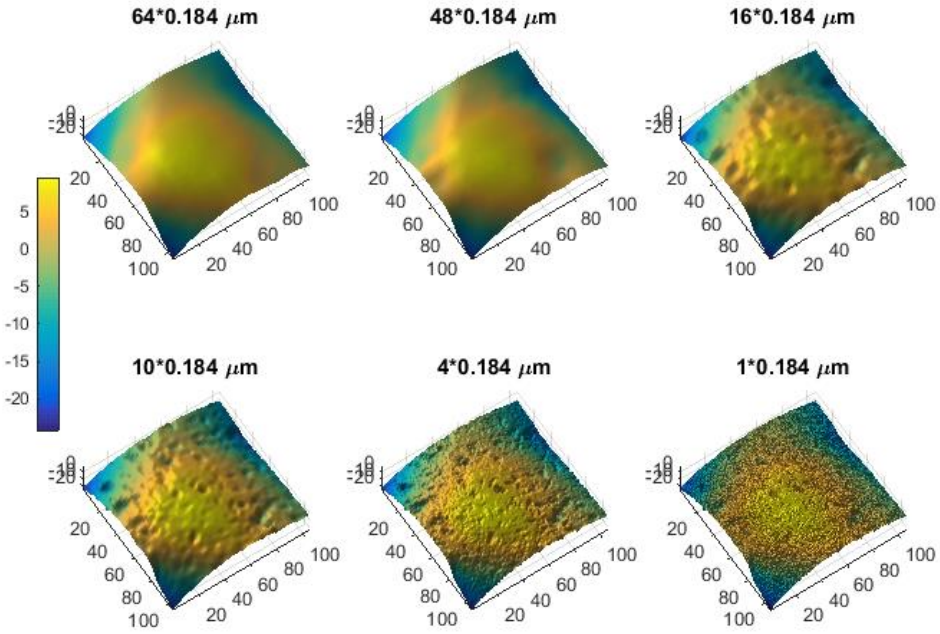

Figure 7 Images of the surface discretized with δ of [64, 48, 16, 10, 4, 1] ×0.184 µm

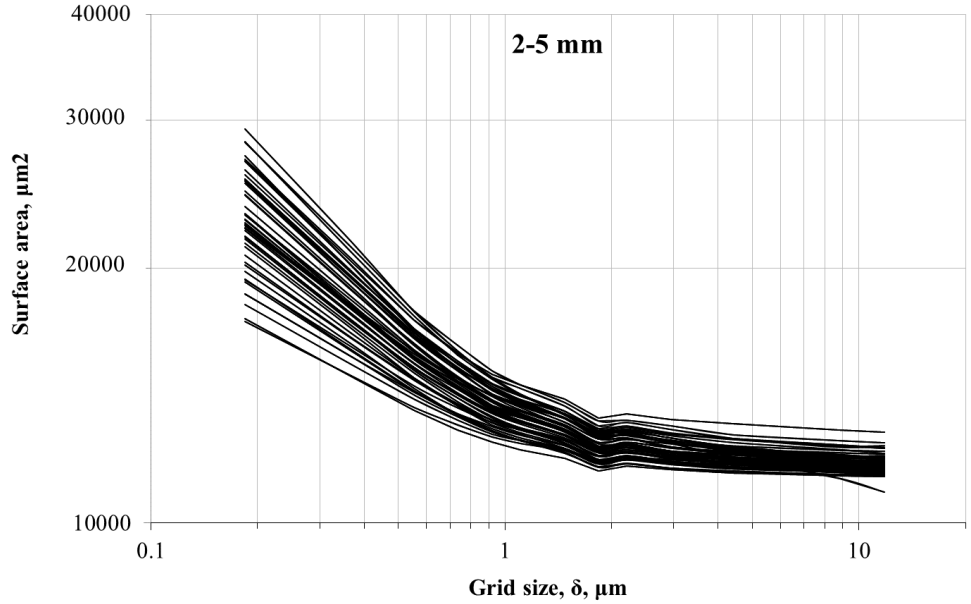

(a)

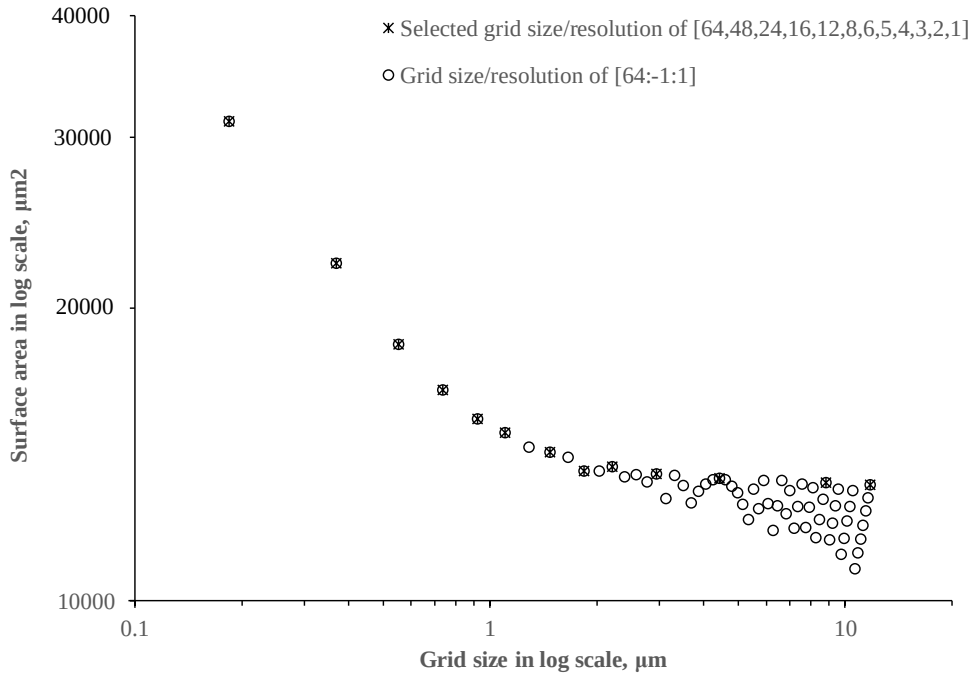

(b)

Figure 8 (a) Estimated surface area for grid sizes δ of [64, 48, 24, 16, 12, 10, 8, 6, 5, 4, 3, 2, 1] ×0.184 µm on a measuring area of 106.6 µm × 106.6 µm for particles of size 2-5 mm, **(b) example of fluctuation with finer discretisation**

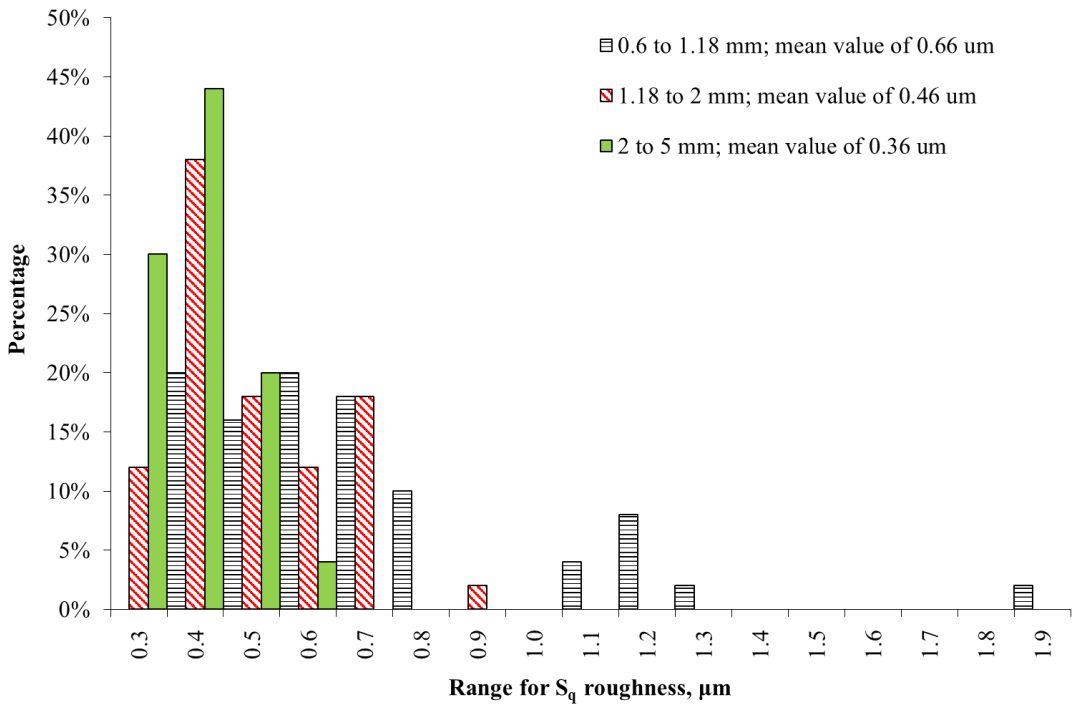

Figure 9 Values of $S_{q,roughness}$ for each size group (50 particles each) with the mean values indicated in the legend

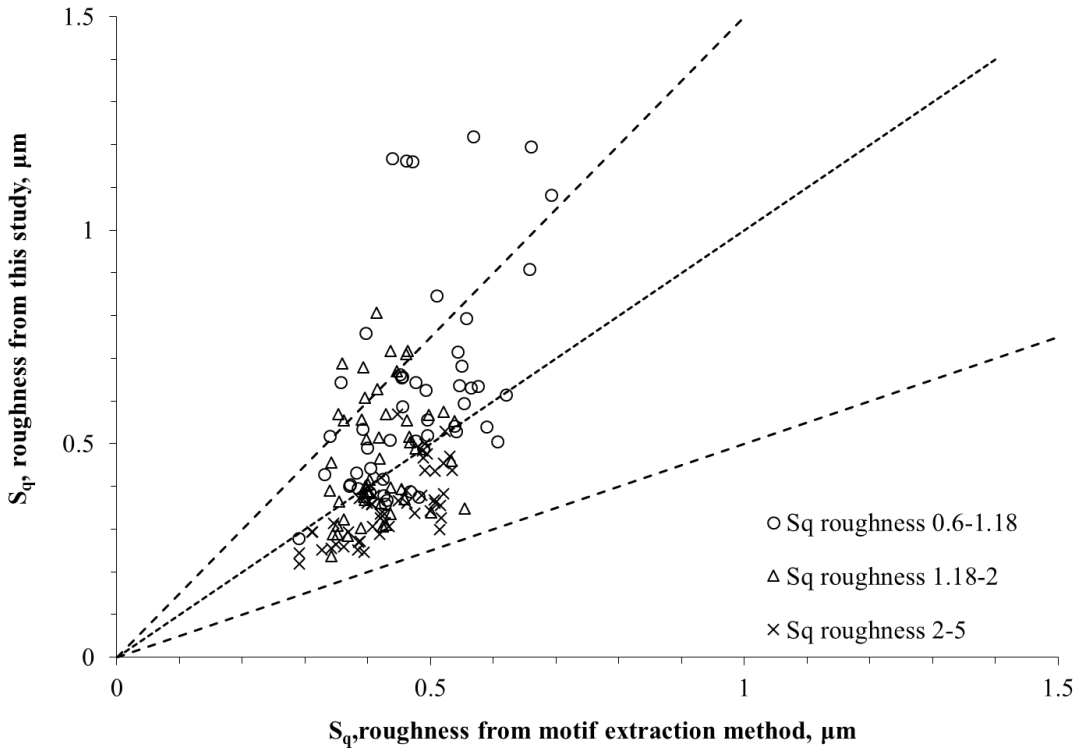

Figure 10 Comparison between the values of $S_{q,roughness}$ obtained from the motif extraction method through the integrated software and the method in this study

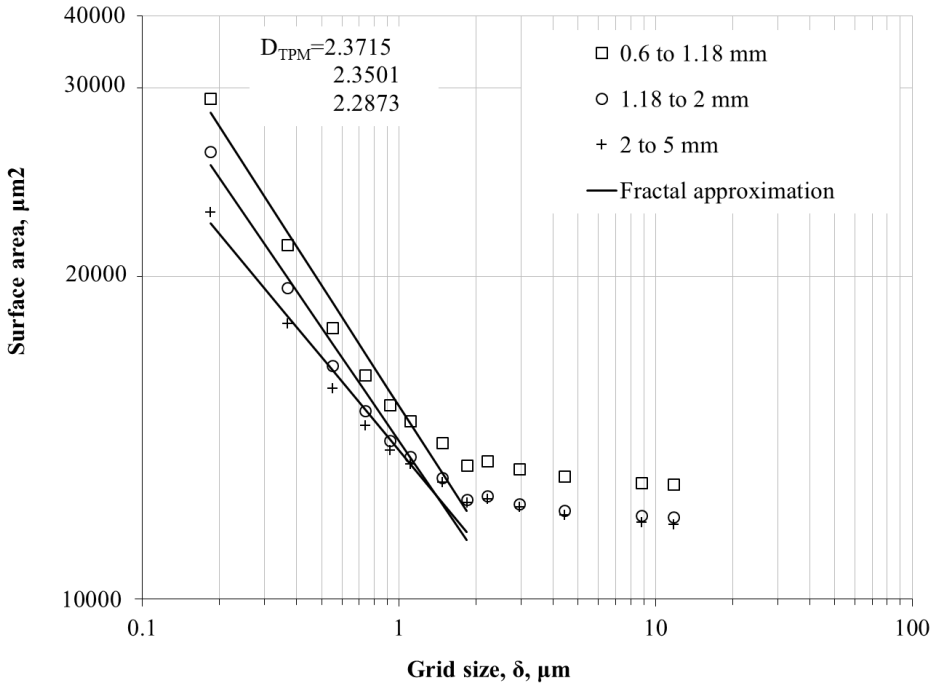

(a)

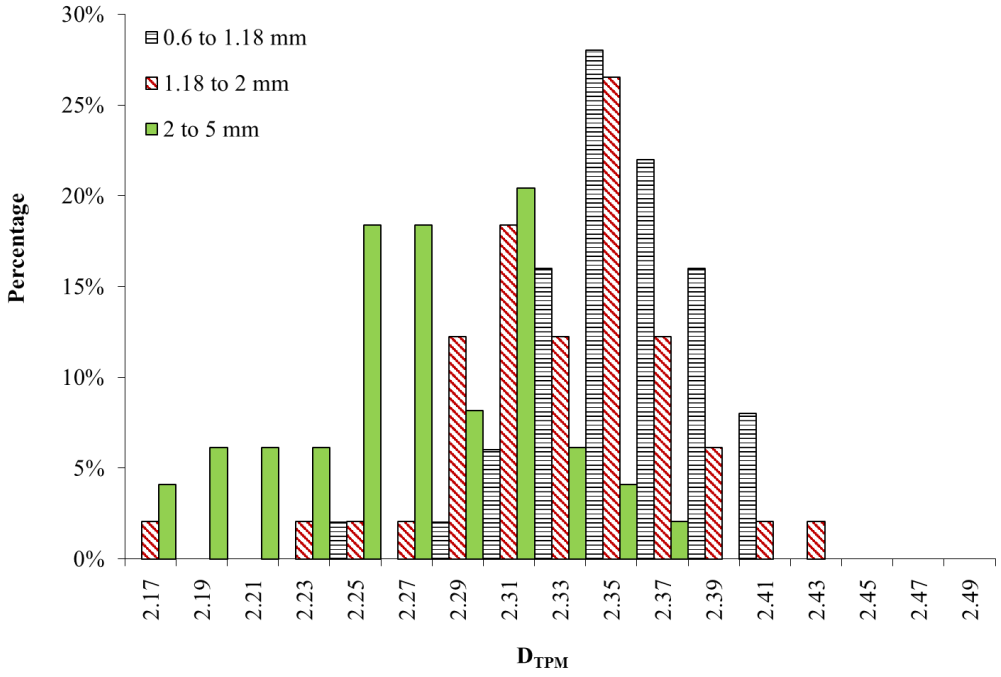

(b)

Figure 11 (a) Average values of estimated surface area with determination of the fractal dimension, (b) distribution of D_{TPM} for each particles size group

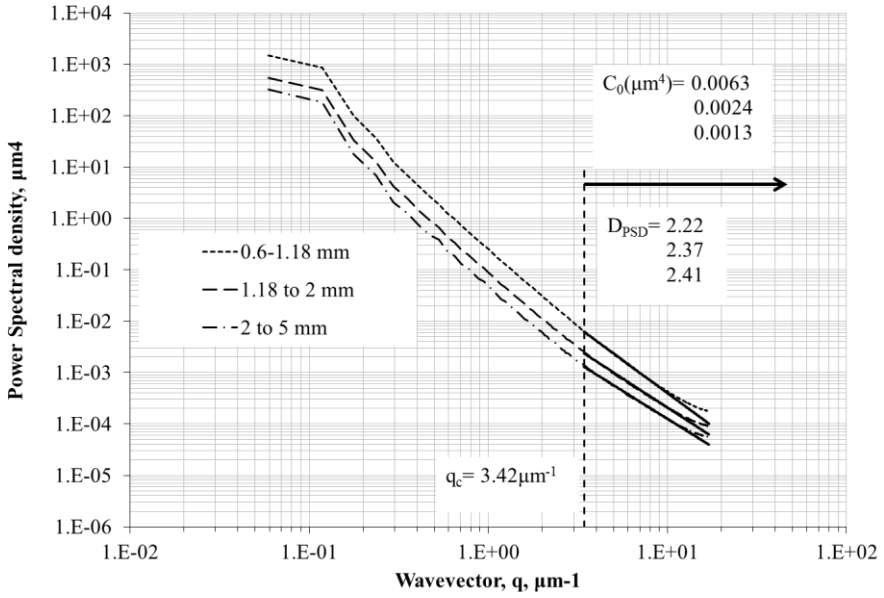

(a)

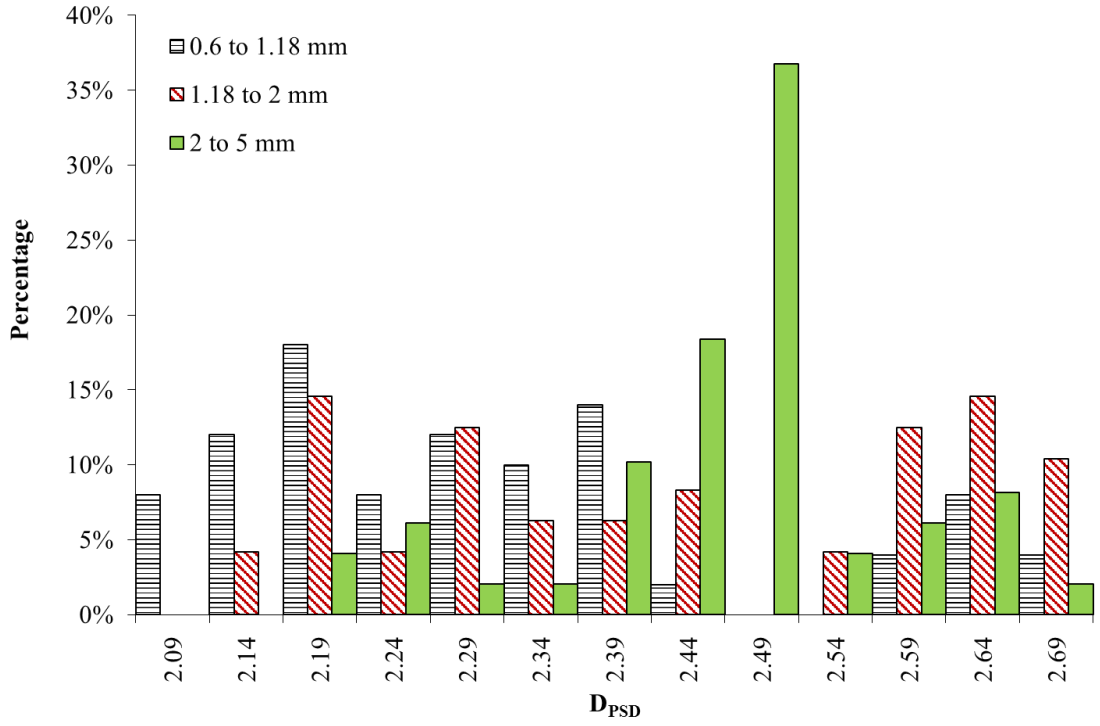

(b)

Figure 12 (a) Average PSDs for each size group together with fractal parameters approximated, (b) distribution of D_{PSD} for each particle size group

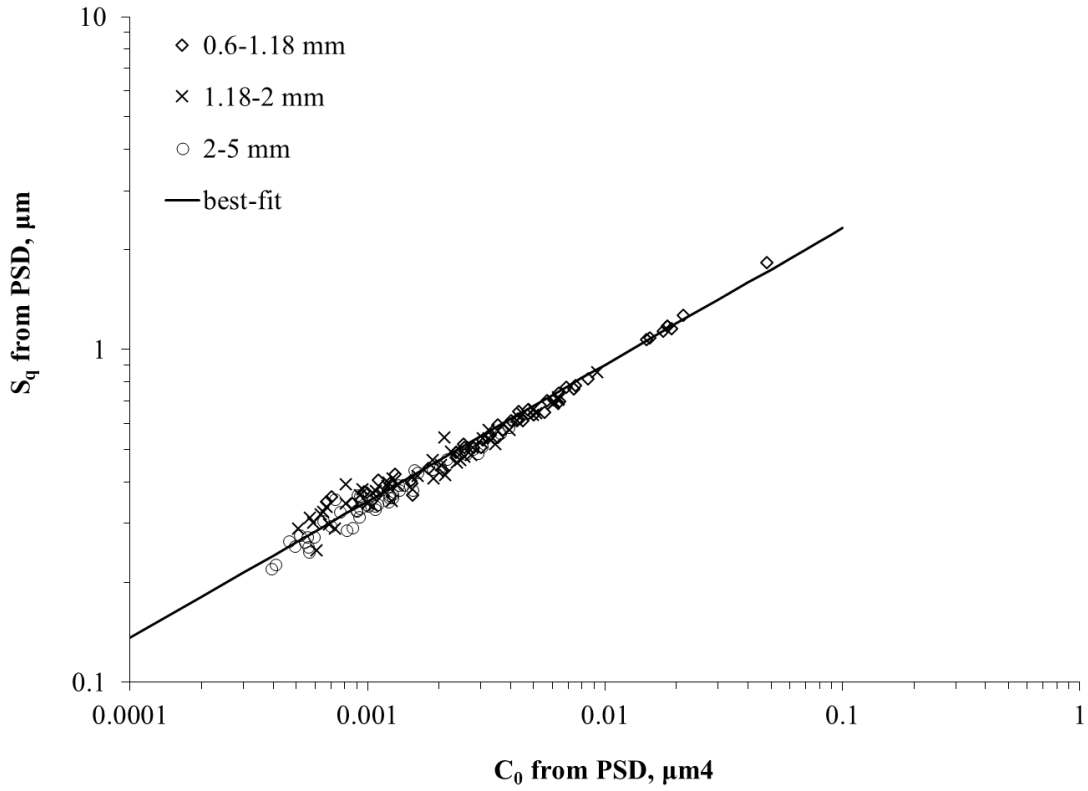

Figure 13 Values of $S_{q,roughness}$ determined from the PSD (Eq. 2) against values of C_0

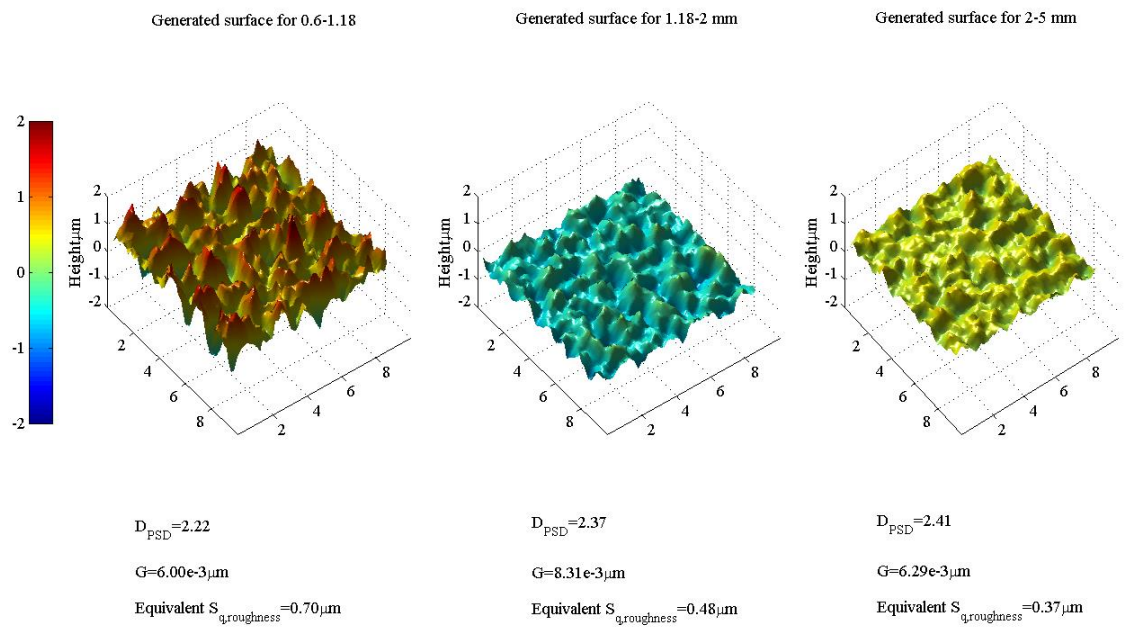

(a)

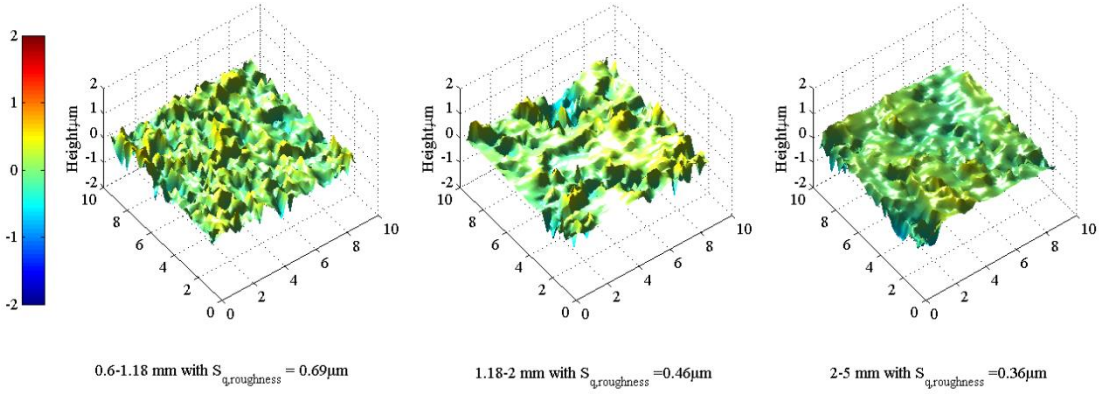

(b)

Figure 14 (a) Generated WM surfaces (9.2 µm × 9.2 µm) average PSD data, (b) measured surfaces for three real particles shown at the same magnification